Vera C. Rubin Observatory
Systems Engineering

Impact of Including Wavelength-dependent PSF Modeling in Rubin Commissioning Data

Aashay Pai, Pierre-Franc.cois Léget, and Chihway Chang

SITCOMTN-174

Latest Revision: 2026-03-06

DRAFT

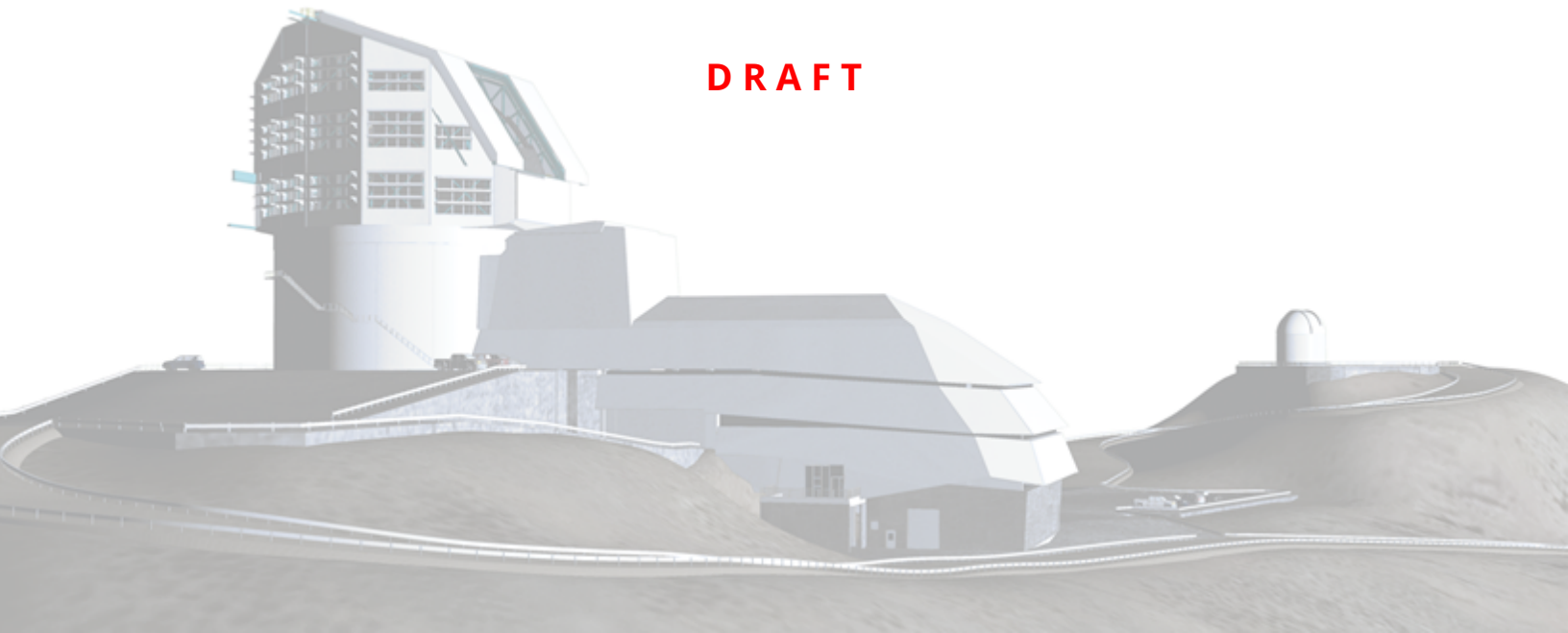

Abstract

We present the results from enabling chromatic modelling of the Point Spread Function (PSF) during the commissioning of the Vera C. Rubin Observatory.

Change Record

Version	Date	Description	Owner name
1	2026-03-04	Added sections 1-6 and section 8	Aashay Pai
1	2026-03-04	Added section 7	Shrihan Agarwal

Document source location: `https://github.com/lsst-sitcom/sitcomtn-174`

Contents

Impact of Including Wavelength-dependent PSF Modeling in Rubin Commissioning Data

1 Introduction

Weak gravitational lensing is one of the key tools in cosmology for understanding the distribution of cosmic structures and deducting the cosmological model that gave rise to it. According to General Relativity, light is bent when it passes through gravitational perturbations sourced by cosmic structure. This means that the light rays from distant galaxies are "lensed" as they travel to us, resulting in small distortions in the observed galaxy shapes. This distortion encodes information of the cosmic structure, allowing us to probe (visible and invisible) cosmic structure.

The central observable in weak lensing is thus the shapes of galaxy images. In particular, we are interested in the galaxy shapes after it has been distorted (or lensed) by the cosmic structure but before it is distorted further by atmospheric or instrumental effects. As this exact quantity is not observable, we can only derive it by having a good model of the atmospheric and instrumental effects, or the Point Spread Function (PSF).

The PSF refers to how a point source will look like on our detectors at a given time and location on the focal plane. It encodes the net effect from the atmosphere, the optics and the detectors and can be thought of as a convolution kernel (or a Green's function) that is applied to the light that comes into the telescope. Having a precise and accurate PSF model for each galaxy is key to the success of weak lensing science for Rubin LSST.

One of the subtleties in modeling the PSF is that the PSF is wavelength-dependent. In particular, Differential Chromatic Refraction (DCR, Sullivan & Reiss, DMTN-017) is the dominating wavelength-dependent PSF effect that exist in ground-based imaging instruments such as Rubin. When we look through the atmosphere at different airmass, the light rays that enter the atmosphere come in a non-perpendicular incident angle and refraction happens at the interface. Blue light refracts more than red light, causing small distortions or displacements of the observed objects that depend on their wavelength. This tech note focuses on this effect and how we could model it in the Rubin pipeline.

The Rubin Observatory uses a PSF fitting strategy adapted from the Dark Energy Survey (DES),

which is based on the PSF in the Full Focal plane (PiFF) algorithm (Jarvis et al., 2021). In this note we examine the performance of the PSF modeling in the Rubin commissioning data. We use the weekly intermittent Data Reduction Pipeline (DRP) w_2025_49 Data.

The structure of this note is as follows. Section 2 describes the DCR effect. Section 3 describes the data products used in this study. Section 4 discusses the fitting procedure, PSF residual definitions and the PSF fitting configuration. Section 5 shows the results of enabling chromatic fitting on PSF residuals. In Section 6 we compare our results with that from DES and in Section 7 propagate the PSF residuals to expected residuals in shear measurements.

2 Differential Chromatic Refraction

As light passes through the Earth's atmosphere, it is refracted toward the zenith. The magnitude of this refraction is wavelength-dependent, with shorter (bluer) wavelengths experiencing stronger refraction than longer (redder) wavelengths. This chromatic dependence leads to small, band-dependent shifts in the measured positions of astronomical objects, which in turn propagate into the modeling of the point-spread function (PSF). Equation 1 defines DCR_1 and DCR_2 as the components of the differential chromatic refraction along the e_1 and e_2 directions, respectively, expressed as functions of the zenith angle z and the parallactic angle q. To compute the DCR, we first determine the local sidereal time for each visit and use it to calculate z and q for every star.

$$\begin{aligned} \mathrm{DCR}_1 &\equiv \tan^2(z)\cos(2q) \\ \mathrm{DCR}_2 &\equiv \tan^2(z)\sin(2q) \end{aligned} \tag{1}$$

3 Data

In this study, we use data products generated by the weekly intermittent Data Reduction Pipelines (DRPs). These DRPs aim to test current data quality and produce LSST-like downstream data from the single-visit exposures. We use two main data products: the object and the refit_psf_star tables.

The object table contains data of stars and galaxies derived from the per-band coadded im-

ages. The `refit_psf_star` table contains data of stars and galaxies derived from the single-visit images and PSF moments modelled with the `PiFF` package (Jarvis et al., 2021).

For measured second-order moments, we use `slot_Shape_xx`, `slot_Shape_yy` and `slot_Shape_xy` that have been measured using the HSM method (Hirata & Seljak, 2003; Mandelbaum et al., 2005, 2018) in which the moments are determined using an iterative elliptical Gaussian fit. For the second-order moments of the `PiFF` PSF model, we use `slot_PsfShape_xx`, `slot_PsfShape_yy` and `slot_PsfShape_xy`, also derived using the HSM shape algorithm.

For star magnitudes, we use calibrated magnitudes (`ap12Flux_mag`) from the `refit_psf_star` table. For magnitudes that are used to calculate colour, we use band-calibrated magnitudes from the `object` tables.

4 PSF Characterization

4.1 Fitting

For a given single-visit image processed by the DRP, the PSF is fit independently on each CCD. Under the default DRP configuration, which does not include chromatic corrections, the PSF modeling is performed using `PiFF`. The input to `PiFF` is a catalog of all detected objects in the image, together with their positions in sky coordinates. From this catalog, `PiFF` selects two subsets of stars: a primary sample used to fit the PSF model and a smaller, reserved sample used for PSF diagnostic tests. A model is then fit to the stellar images to obtain a maximum-likelihood estimate of the PSF parameters (position, and optionally, wavelength) at each stellar location. Finally, the fitted model parameters are interpolated across the stellar sample to estimate the PSF over the full focal plane using a second order polynomial. To incorporate colour dependence in the PSF modeling, we provide `PiFF` with stellar colours derived using the Forward Global Calibration Method (FGCM; Burke et al., 2018), which are computed in a preceding step of the DRP.

4.2 PSF Shape Definitions

Equation 2 shows the definitions for PSF size (T) and ellipticity (e_1 & e_2) that are used in this work.

$$\begin{aligned} T &\equiv i_{xx} + i_{yy} \\ e_1 &\equiv \frac{i_{xx} - i_{yy}}{i_{xx} + i_{yy}} \\ e_2 &\equiv \frac{2i_{xy}}{i_{xx} + i_{yy}} \end{aligned} \tag{2}$$

For each quantity above (T, e_1, e_2), we also define the residual to be the difference between the measured value and the fit value of the model: $\delta X \equiv X_{\text{PSF}} - X_{\text{model}}$ and $\delta X/X \equiv (X_{\text{PSF}} - X_{\text{model}})/X_{\text{PSF}}$.

4.3 PSF Fitting Configuration

We test several `PiFF` chromatic fitting configurations to minimize the error in the PSF model due to chromatic effects. We saw most improvement in the PSF fit by using a 2nd-order polynomial fit in spatial position and colour, with no significant improvement from using higher orders. The final configuration is shown below.

```
config.psf_determiner['piff'].spatialOrderPerBand = {
  "u": 2, "g": 2, "r": 2, "i": 2, "z": 2, "y": 2,
}
config.psf_determiner['piff'].zerothOrderInterpNotEnoughStars = False
config.psf_determiner['piff'].piffBasisPolynomialSolver = "cpp"
config.psf_determiner['piff'].piffPixelGridFitCenter = False
config.psf_determiner['piff'].useColor = True
config.psf_determiner['piff'].colorOrder = 2
config.psf_determiner['piff'].color = {
  "u": "g-i", "g": "g-i", "r": "g-i", "i": "g-i",
  "z": "i-z", "y": "i-z",
}
```

5 Results

In this section, we study PSF size and ellipticity residuals as a function of magnitude, sky position (DCR), and colour. We use the week 49 DRP data, which contains 4898 visits and ∼ 153 million star measurements. We perform the measurements using all stars, and we use stars binned by $r - z$ colour in 3 equally distributed bins to quantify the colour-dependent effects. We show how the PSF model improves when enabling chromatic fitting of the PSF in `PiFF`.

5.1 Residuals by magnitude

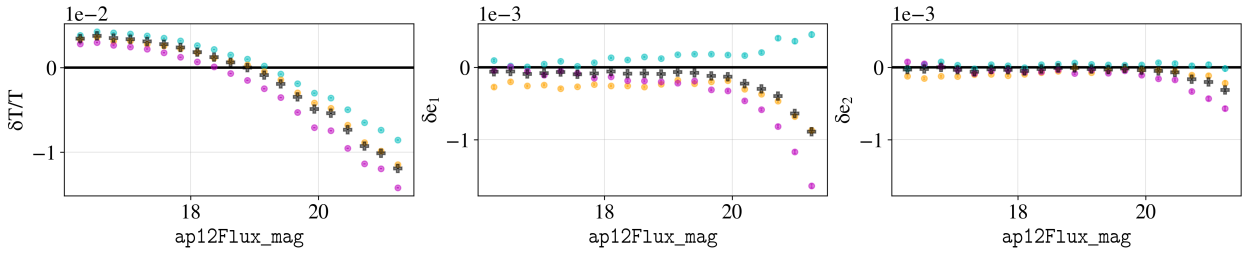

(a) without chromatic PSF fitting.

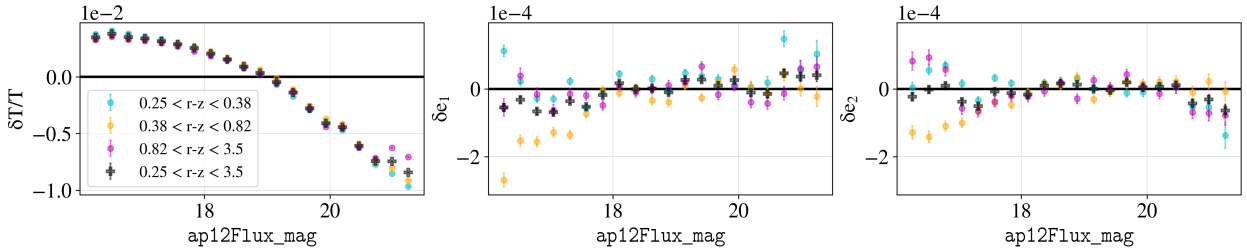

(b) with chromatic PSF fitting.

Figure 1: PSF $\delta T/T$, δe_1 and δe_2 as a function of `ap12Flux_mag` before (a) and after (b) turning on chromatic PSF fitting. Note that the y-axis range in (a) and (b) are different. Stars are divided into equal-sized colour bins of $r - z \in [0.25, 0.38, 0.82, 3.5]$. Enabling chromatic PSF reduces the spread or residuals between colour bins.

Figure 1 shows the PSF $\delta T/T$, δe_1 and δe_2 residuals as a function of star magnitude. The stars have been divided into colour bins of $r - z \in [0.25, 0.38, 0.82, 3.5]$. Without chromatic fitting, the spread in δe_1 at the faint end is $\sim 3\times$ larger than that of δe_2. Enabling chromatic fitting of the PSF tightens and thereby reduces the spread in the residuals toward the faint end in all colour bins, but is most prominently seen in δe_1. As expected, the magnitude of the errors are not reduced by chromatic fitting, but the spread between the individual colour bins is reduced, which can be most clearly seen in $\delta T/T$.

Figure 2 shows the residuals of PSF $\delta T/T$, δe_1 and δe_2 as a function of star magnitude for visits in the g band only, where we expect to see the most significant chromatic PSF effect. The stars are divided into colour bins of $r - z \in [0.24, 0.35, 0.57, 3.5]$. Enabling chromatic fitting reduces $\delta T/T$ residuals by $\sim$ 50%. For δe_1 and δe_2, chromatic fitting tightens the residuals at the faint end (mag > 18) by $\sim$ 75%. It is comparatively ineffective in tightening the reddest colour bin at the bright end.

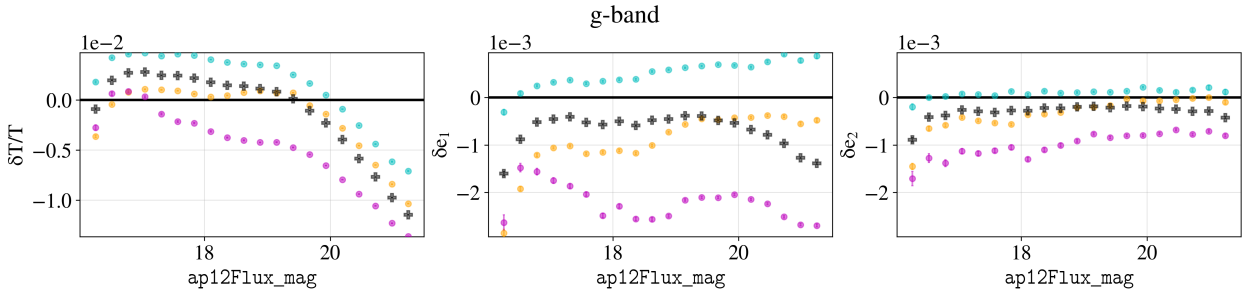

(a) without chromatic PSF fitting.

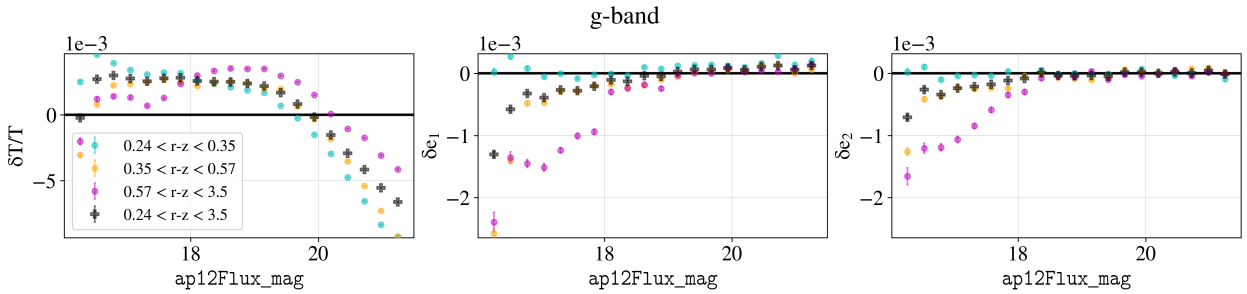

(b) with chromatic PSF fitting.

Figure 2: PSF $\delta T/T$, δe_1 and δe_2 for g band visits only as a function of `ap12Flux_mag` before (a) and after (b) turning on chromatic PSF fitting. Note that the y-axis range in (a) and (b) are different. Stars are divided into equal-sized colour bins of $r - z \in [0.24, 0.35, 0.57, 3.5]$. Enabling chromatic PSF shows the most improvement in the residuals in the blue, faint objects.

5.2 Residuals by colour

Figure 3 plots the PSF $\delta T/T$, δe_1 and δe_2 residuals as a function of $g - i$ colour. The right-most panel of subfig. 3b shows the number density of stars as a function of $g - i$ colour, which is common to both subfigures. The residuals of $\delta T/T$ and δe_1 show the strongest colour dependence in the u and g bands respectively. Chromatic fitting corrects the colour dependence in the g band, but is ineffective in correcting the u band colour dependence. However, this could be due to the lack of enough objects in the u band in red $g - i$ bins, as can be seen in the histogram. The discrepancy between the magnitude of δe_1 and δe_2 residuals is also unclear.

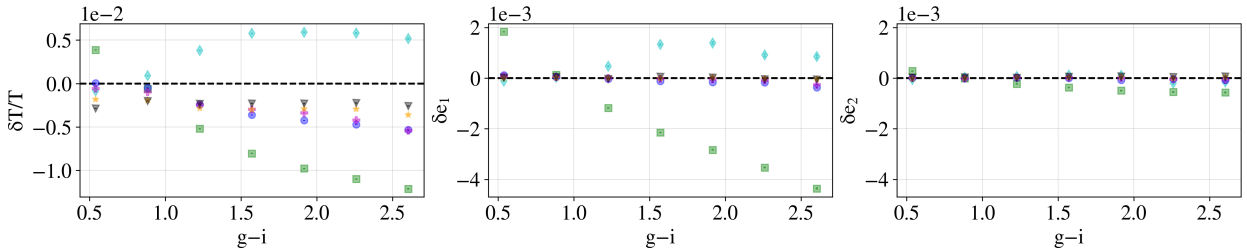

(a) without chromatic PSF fitting.

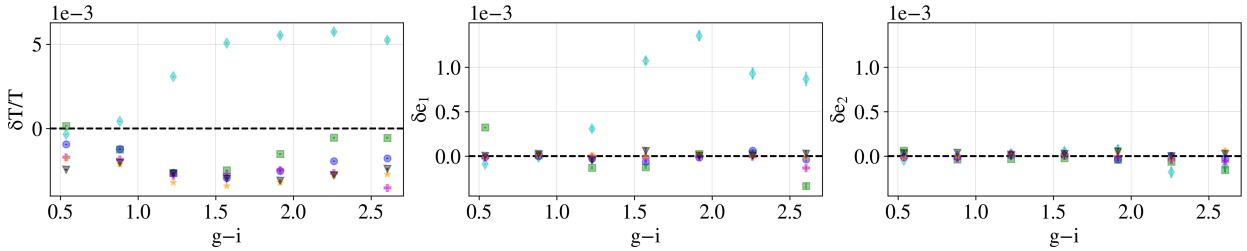

(b) with chromatic PSF fitting.

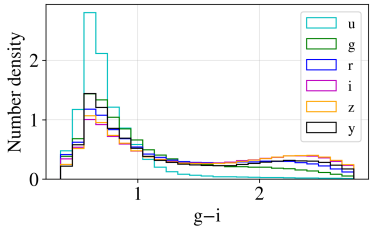

(c) Number density as a function of $g - i$ colour.

Figure 3: PSF $\delta T/T$, δe_1 and δe_2 as a function of $g - i$ colour. The u and g band residuals show the highest dependence on $g - i$ colour. Note that the y-axis range in (a) and (b) are different. Enabling chromatic fitting corrects the g band colour dependence, but is unable to correct the u band dependence, possibly due to the small number of observations with red $g - i$ colour.

5.3 Residuals by Position (DCR)

Figure 4 shows the PSF δe_1 and δe_2 as a function of DCR_1 and DCR_2 respectively for observations in the g band, which is affected the most by DCR. The stars are separated in colour bins of $r - z \in [0.25, 0.38, 0.82, 3.5]$. Chromatic fitting of the PSF corrects DCR dependent residuals by up to $\sim$ 90% in δe_1 and up to $\sim$ 95% in δe_2, therefore reducing DCR dependent errors by almost an order of magnitude.

Figure 5 shows the PSF δe_1 and δe_2 as a function of DCR_1 and DCR_2 respectively for observations in the r band. The stars are separated in colour bins of $r - z \in [0.25, 0.38, 0.82, 3.5]$. Chromatic fitting of the PSF corrects DCR dependent residuals by up to $\sim$ 50% in δe_1 and δe_2.

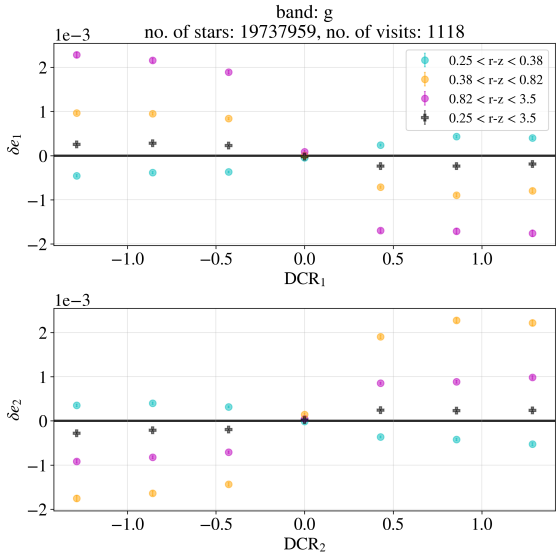

(a) without chromatic PSF fitting.

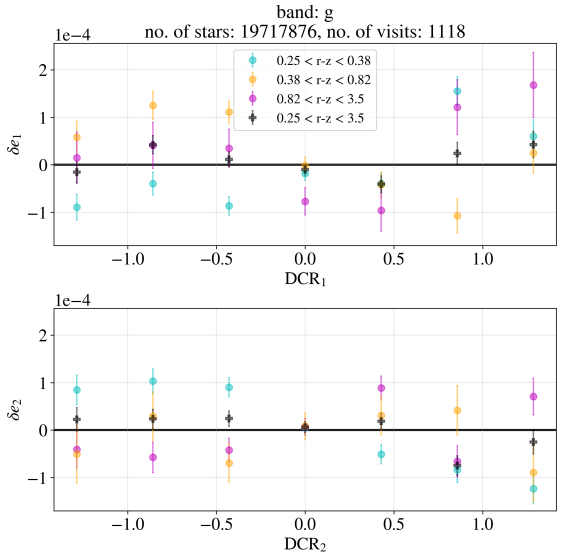

(b) with chromatic PSF fitting.

Figure 4: PSF δe_1 and δe_2 as a function of DCR_1 and DCR_2 respectively before (a) and after (b) turning on chromatic PSF fitting. Note that the y-axis range in (a) and (b) are different. Chromatic fitting of the PSF reduces residuals by up to $\sim 95\%$ in the g-band.

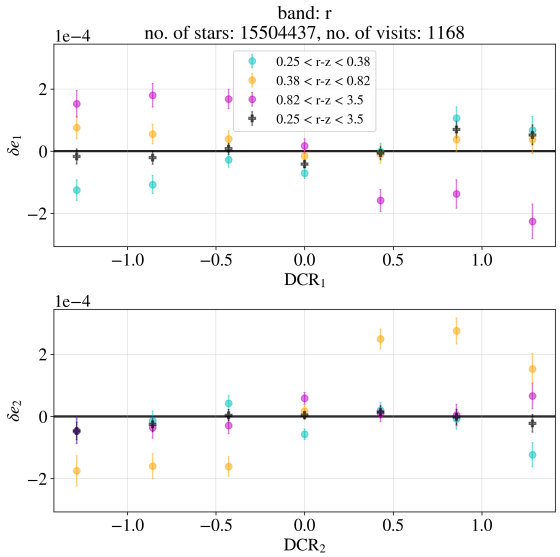

(a) without chromatic PSF fitting.

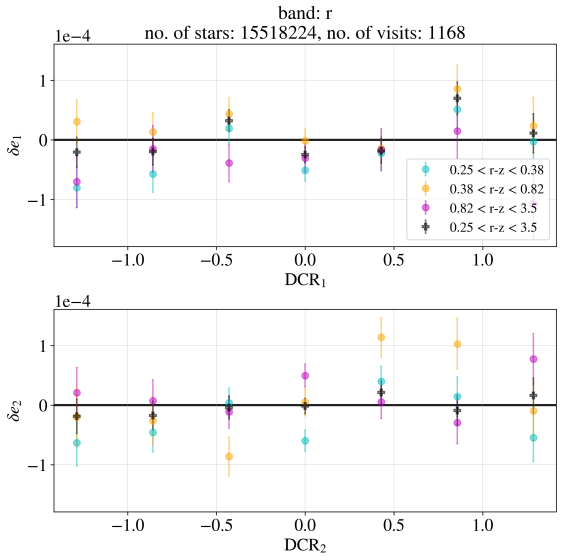

(b) with chromatic PSF fitting.

Figure 5: PSF δe_1 and δe_2 as a function of DCR_1 and DCR_2 respectively before (a) and after (b) turning on chromatic PSF fitting. Note that the y-axis range in (a) and (b) are different. Chromatic fitting of the PSF reduces residuals by up to $\sim$50% in the r-band.

6 Comparison to the Dark Energy Survey

The Dark Energy Survey (DES) was a six-year optical and near-infrared imaging survey designed to investigate the origin of cosmic acceleration. DES operated from 2013 to 2019 using the Dark Energy Camera (DECam) mounted on the 4 m Victor M. Blanco Telescope at Cerro Tololo Inter-American Observatory in Chile. DECam, the camera used to conduct the survey, is a 570-megapixel wide-field imager with a $\sim$ 3 deg^2 field of view, consisting of 62 science CCDs. The survey imaged approximately 5000 deg^2 of the southern sky in five broadband filters ($grizY$) to a typical depth of $i \approx 24$ mag (10σ for galaxies).

The PSF pipelines used by the Rubin Observatory are modelled after the DES pipelines, including the use of the same PSF modelling software: `PiFF`. As the two surveys share similar science goals, we compare current Rubin Observatory PSF characteristics to DES Year 6 PSF results (Schutt et al., 2025). The DES Y6 PSF star sample consists of $\sim$ 110 million stars, while the Rubin week 49 DRP data contains $\sim$ 153 million stars.

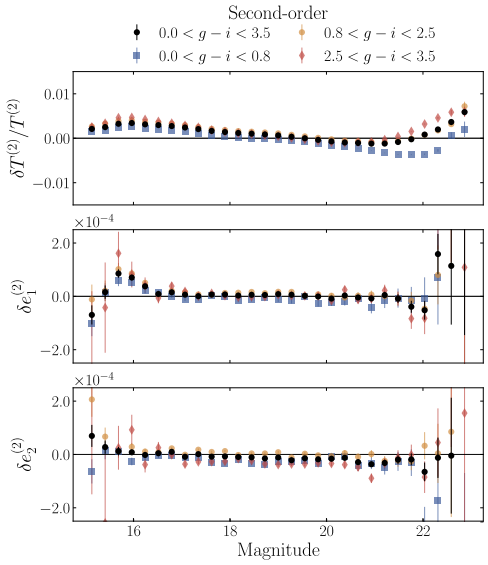

Figure 6: DES Y6 PSF $\delta T/T$, δe_1 and δe_2 as a function of magnitude. Stars are divided into equal-sized colour bins of $g - i \in [0.0, 0.8, 2.5, 3.5]$.

Figure 6 shows the dependence of chromatically-fitted PSF $\delta T/T$, δe_1 and δe_2 residuals on magnitude in DES Y6 data. Comparing the residuals to Fig. 1b, we find that the magnitude of `PiFF` residuals are on par with DES levels, even though the overall trend looks different.

Figure 7 shows the DES Y6 PSF residuals as a function of $g - i$ and $i - z$ colour. Comparing

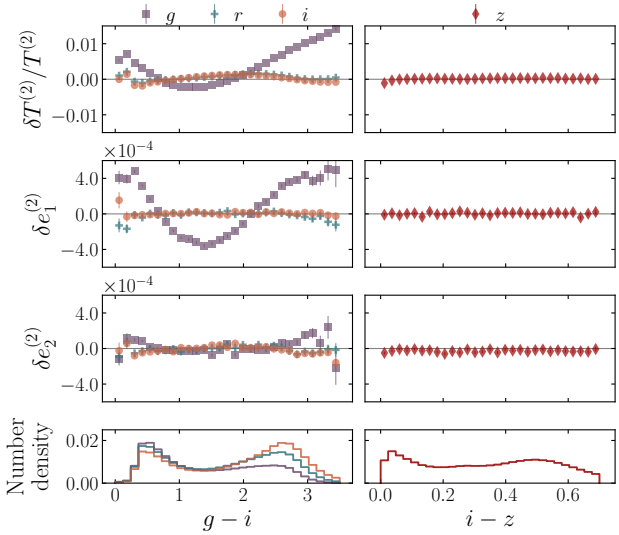

Figure 7: DES Y6 residuals as a function of $g-i$ colour (for the gri bands) and $i-z$ colour (for the z band).

the colour dependence to Fig. 3b, DES Y6 g band $\delta T/T$ residuals are up to $\sim$ 50% larger than Rubin.

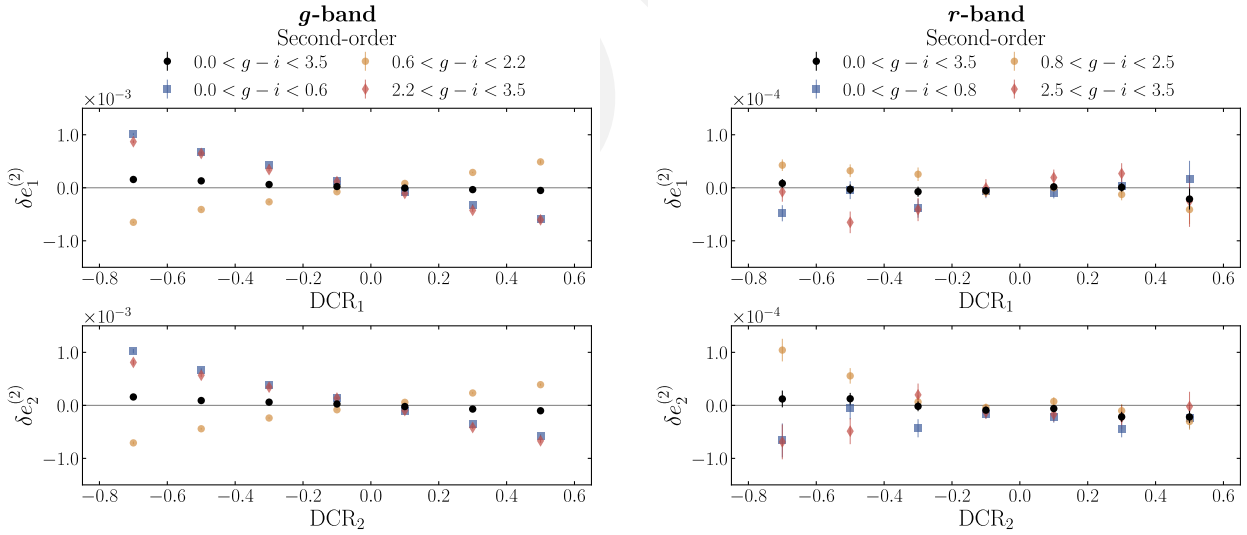

Figure 8: DES Y6 PSF δe_1 and δe_2 as a function of DCR_1 and DCR_2 respectively, in the g and r bands.

Figure 8 shows the DES Y6 ellipticity residuals as a function of DCR_1 and DCR_2 in the g and r bands. Comparing these to Fig. 4b and Fig. 5b, we find that in the Rubin data, the PSF model

errors coming from DCR is $\sim 80\%$ better than that in DES Y6 in the g band and to similar levels in the r band.

7 Impact on Shear Systematics

Systematics due to DCR propagate to the cosmic shear measurement through PSF modeling errors. These errors are additive and the subset of them due to DCR can typically be represented as,

$$\gamma_{\rm obs} = \gamma_{\rm true} + \beta \delta \mathbf{e}^{\rm DCR}$$

to second order, following Gatti et al. (2021), where β is an empirically estimated quantity that is typically of order unity. Therefore, ignoring chance correlations $\langle \gamma_{\rm true} \delta \mathbf{e}^{\rm DCR} \rangle$, the impact on the cosmic shear is approximately,

$$\langle \gamma_{\rm obs} \gamma_{\rm obs} \rangle \approx \langle \gamma_{\rm true} \gamma_{\rm true} \rangle + \beta^2 \langle \delta \mathbf{e}^{\rm DCR} \delta \mathbf{e}^{\rm DCR} \rangle.$$

In practice, we can forecast this impact as follows. We set $\beta = 1$ as it is typically of order unity. As shown in Figure 4 & 5, the $\delta \mathbf{e}^{\rm DCR}$ due to DCR is determined empirically using stars as diagnostics. The values $\rm DCR_1$ and $\rm DCR_2$ themselves can also be determined from the time, RA and Dec of observation and through Equation 1. From the LSST survey scheduler OpSim Baseline v5.1.0, we find this information for each exposure, calculate and tile the DCR values across the exposure field of view (approximated as a circle of radius 1.75°), and finally aggregate them into a HEALPix map of the sky weighted by the effective exposure time $T_{\rm eff}$×visitExposureTime. This is shown in Figure 9.

DCR is a function of the color difference between the average PSF star and galaxies. Therefore, higher redshift galaxies that are redder have greater DCR effect. We estimate the average range of source galaxy colors in LSST redshift bins using galaxies from DES. To do so, we draw galaxies from the DES into LSST redshift bins and use their color distribution for LSST. Given that LSST goes to higher redshifts than DES, this works for all but the last redshift bin. For this bin, we linearly extrapolate the galaxy colors out to high redshift. This assumption is likely

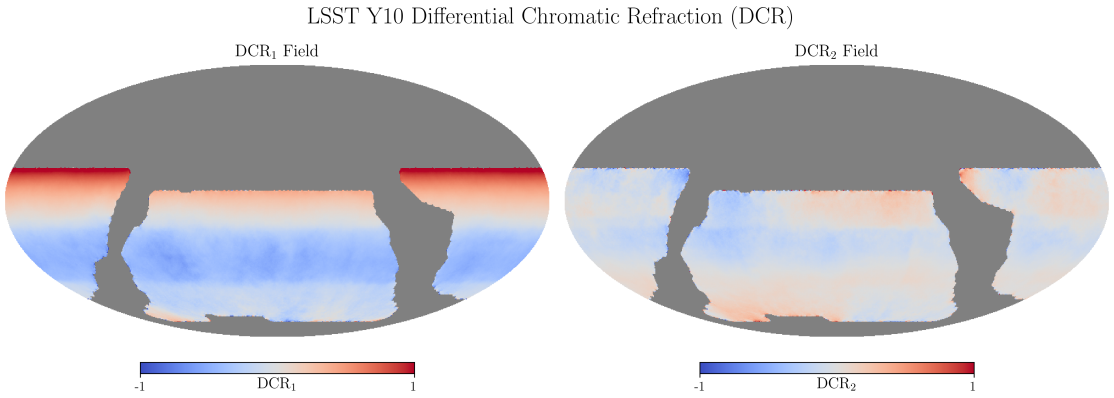

Figure 9: Differential Chromatic Refraction maps for LSST Y10 WFD using OpSim Baseline v5.1.0.

the largest source of inaccuracy in this forecast, as the slope of the DCR – e relation itself is sensitive to the $r-z$ color of the galaxies. Additionally, as the Balmer break shifts out of the z-band at $z \approx 1.5$, it is unlikely that the galaxy colors increase linearly. However, for a worst-case forecast, this is a reasonable assumption.

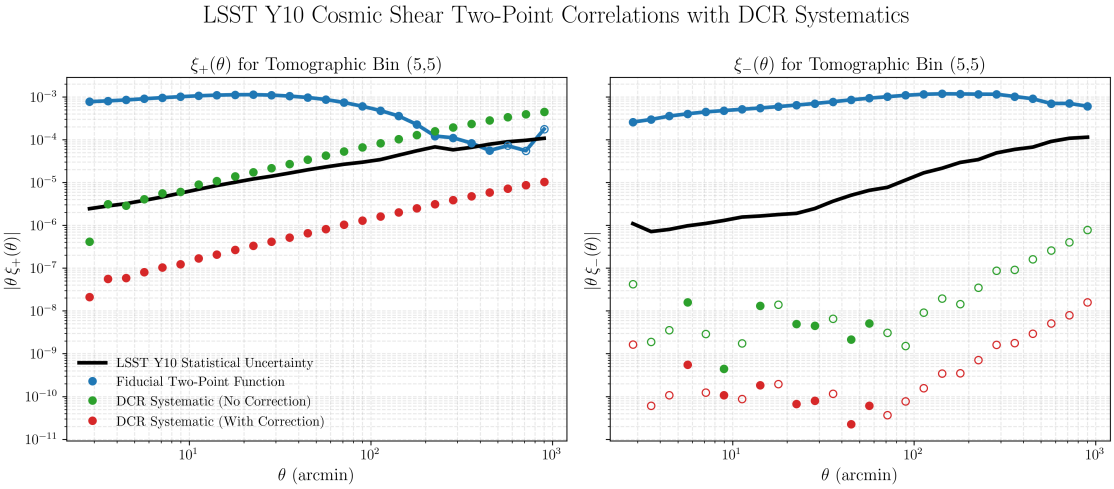

Figure 10: Impact of DCR on the cosmic shear two-point correlation function. In blue, we show the fiducial cosmic shear for the most impacted tomographic bin autocorrelation (5, 5). The black line represents the statistical jackknife uncertainty of cosmic shear, as a baseline. The DCR Systematic $\langle \delta\mathbf{e}^{\rm DCR} \delta\mathbf{e}^{\rm DCR} \rangle$ if uncorrected (shown in green) is comparable to or larger than LSST Y10 statistical uncertainty for ξ_+. The corrected DCR signal shown in red sufficiently reduces this effect by two orders of magnitude.

Finally, we linearly fit the color-dependent DCR-δe relation for the uncorrected and corrected chromatic PSF case, and apply it to the DCR maps (Figure 9). To calculate the two-point corre-

lation function of this error map, we use the `treecorr` software (Jarvis et al., 2004). We create a catalog from pixels, and perform the correlation $\langle \delta \mathbf{e}^{\mathrm{DCR}} \delta \mathbf{e}^{\mathrm{DCR}} \rangle$ for a range from 2.5 to 1000 arcmin, with 26 bins (to mimic DES within its range), and a `bin_slop` of 0.1. To forecast the shear signal and uncertainty, we use `GLASS` (Tessore et al., 2023), alongside the redshift distributions forecast by the LSST Science Requirements Document (The LSST Dark Energy Science Collaboration et al., 2018) and `treecorr` to estimate the jackknife uncertainty. The results are shown in Figure 10.

We find that the DCR systematic has a non-negligible impact on ξ_+, where for Y10 of the LSST survey, systematic uncertainties would have been comparable to statistical uncertainties if uncorrected. Correcting for the chromatic PSF using PiFF color-dependence sufficiently reduces this systematic by 2 orders of magnitude, and may become more accurate as the survey progresses. Even post-correction, we note that on large scales $\theta \gtrsim 300$ arcmin, where the statistical uncertainty is dominated by cosmic variance, DCR systematics approach 10% of cosmic shear ξ_+ (and statistical uncertainty). However, since the statistical uncertainty dominates, this does not affect cosmological measurement. For ξ_-, the impact from DCR is negligible. Further detailed study of the forecasted impact of DCR and other shape systematics for LSST will be presented in Agarwal et al. (in prep).

8 Conclusions

In this note, we have evaluated the impact of enabling chromatic PSF modeling during commissioning of the Vera C. Rubin Observatory using weekly DRP data (`w_2025_49`). By incorporating colour-dependent terms into the `PiFF` PSF model, we directly address wavelength-dependent effects, in particular Differential Chromatic Refraction (DCR), which is expected to be one of the dominant chromatic systematics in ground-based weak lensing measurements.

Using ∼153 million stellar measurements across 4898 visits, we have shown that enabling a second-order polynomial dependence in both spatial position and colour substantially improves PSF residuals:

- **Residuals vs. magnitude:** Chromatic fitting significantly reduces the spread in PSF size and ellipticity residuals between colour bins, particularly in the faint regime. In the g band, where DCR is strongest, residuals in $\delta T/T$ decrease by ∼50%, and faint-end ellipticity residuals tighten by up to ∼75%.

- **Residuals vs. colour:** The strong colour dependence observed in the non-chromatic configuration is largely mitigated in the g band when chromatic fitting is enabled. Remaining trends in the u band are likely driven by limited stellar statistics in the reddest colour bins rather than fundamental modeling limitations.
- **Residuals vs. DCR:** The most dramatic improvement is seen in DCR-dependent trends. In the g band, chromatic PSF modeling reduces DCR-correlated ellipticity residuals by up to ∼90–95%, effectively suppressing these systematics by nearly an order of magnitude. Improvements in the r band are more modest (∼50%) but still significant.

When compared to Dark Energy Survey (DES) Year 6 results, Rubin commissioning data with chromatic PSF fitting achieves residual levels that are comparable to, and in some cases improved relative to, DES. In particular, DCR-dependent ellipticity residuals in the g band are suppressed to levels that outperform DES by up to ∼80%, demonstrating that the Rubin PSF modeling framework is already competitive at the commissioning stage.

Finally, we propagated DCR-induced PSF residuals to forecasts of cosmic shear systematics. Without chromatic correction, the induced additive systematic $\langle \delta e_{\rm DCR}\, \delta e_{\rm DCR} \rangle$ can be comparable to or exceed the expected LSST Year 10 statistical uncertainty in the most affected tomographic bins. With chromatic PSF modeling enabled, this contribution is reduced by approximately two orders of magnitude, bringing the DCR-induced shear systematic well below the statistical error budget across relevant angular scales.

A Acknowledgements

This material is based upon work supported in part by the National Science Foundation through Cooperative Agreements AST-1258333 and AST-2241526 and Cooperative Support Agreements AST-1202910 and AST-2211468 managed by the Association of Universities for Research in Astronomy (AURA), and the Department of Energy under Contract No. DE-AC02-76SF00515 with the SLAC National Accelerator Laboratory managed by Stanford University. Additional Rubin Observatory funding comes from private donations, grants to universities, and in-kind support from LSST-DA Institutional Members.

B References

Agarwal, S., Chang, C., Giannini, G., Anbajagane, D., Drlica-Wagner, A., in prep, Impact of spatially varying systematic effects on shape measurements and cosmology: a study for des, decade and lsst,
In preparation

Burke, D.L., Rykoff, E.S., Allam, S., et al., 2018, AJ, 155, 41 (arXiv:1706.01542), doi:10.3847/1538-3881/aa9f22, ADS Link

Gatti, M., Sheldon, E., Amon, A., et al., 2021, MNRAS, 504, 4312 (arXiv:2011.03408), doi:10.1093/mnras/stab918, ADS Link

Hirata, C., Seljak, U., 2003, MNRAS, 343, 459 (arXiv:astro-ph/0301054), doi:10.1046/j.1365-8711.2003.06683.x, ADS Link

Jarvis, M., Bernstein, G., Jain, B., 2004, Monthly Notices of the Royal Astronomical Society, 352, 338, doi:10.1111/j.1365-2966.2004.07926.x

Jarvis, M., Bernstein, G.M., Amon, A., et al., 2021, MNRAS, 501, 1282 (arXiv:2011.03409), doi:10.1093/mnras/staa3679, ADS Link

Mandelbaum, R., Hirata, C.M., Seljak, U., et al., 2005, MNRAS, 361, 1287 (arXiv:astro-ph/0501201), doi:10.1111/j.1365-2966.2005.09282.x, ADS Link

Mandelbaum, R., Lanusse, F., Leauthaud, A., et al., 2018, MNRAS, 481, 3170 (arXiv:1710.00885), doi:10.1093/mnras/sty2420, ADS Link

Schutt, T., Jarvis, M., Roodman, A., et al., 2025, The Open Journal of Astrophysics, 8, 26 (arXiv:2501.05781), doi:10.33232/001c.132299, ADS Link

[DMTN-017], Sullivan, I.S., Reiss, D.J., 2015, *Differential Chromatic Refraction: literature overview*, Data Management Technical Note DMTN-017, NSF-DOE Vera C. Rubin Observatory, URL https://dmtn-017.lsst.io/

Tessore, N., Loureiro, A., Joachimi, B., von Wietersheim-Kramsta, M., Jeffrey, N., 2023, The Open Journal of Astrophysics, 6, 11 (arXiv:2302.01942), doi:10.21105/astro.2302.01942, ADS Link

The LSST Dark Energy Science Collaboration, Mandelbaum, R., Eifler, T., et al., 2018, arXiv e-prints, arXiv:1809.01669 (arXiv:1809.01669), doi:10.48550/arXiv.1809.01669, ADS Link

C Acronyms

Acronym	Description
AST	NSF Division of Astronomical Sciences
AURA	Association of Universities for Research in Astronomy
CCD	Charge-Coupled Device
DCR	Differential Chromatic Refraction
DE-AC02	Department of Energy contract number prefix
DECam	Dark Energy Camera
DES	Dark Energy Survey
DMTN	DM Technical Note
DRP	Data Release Processing
FGCM	Forward Global Calibration Method
HEALPix	Hierarchical Equal-Area iso-Latitude Pixelisation
HSM	Hierarchical Storage Management
LSST	Legacy Survey of Space and Time (formerly Large Synoptic Survey Telescope)
LSST-DA	LSST Discovery Alliance
OpSim	Operations Simulation
PSF	Point Spread Function
RA	Rapid Analysis
SI	System and Information Integrity
SLAC	SLAC National Accelerator Laboratory
WFD	Wide-Fast-Deep